Supplemental Information

A semi-analytical decomposition analysis of surface plasmon generation and the optimal nanoledge plasmonic device

Zheng Zeng,[a] Madu N. Mendis,[b] David H. Waldeck,[b] and Jianjun Wei*[a]

[a]Department of Nanoscience, Joint School of Nanoscience and Nanoengineering, University of North Carolina at Greensboro, Greensboro, NC 27401, USA. j_wei@uncg.edu

[b]Department of Chemistry, University of Pittsburgh, Pittsburgh, PA 15260, USA.

Semi-analytical analysis:

For the plane-wave basis, the magnetic field below the slit H(y,z) can be written as[1-3]

$$H_{below-slit}(y,z) = (N_p)^{-1/2}\exp(-ikn_1z) + \int_{-\infty}^{\infty} dur_u \exp(ikn_1uy)\exp(ikn_1vz), \quad (S1)$$

where r_u is the plane-wave reflection coefficients, and u and v are applied for numerical integration with $u^2+v^2=1$.

Meanwhile, the magnetic field inside the slit H(y,z) could also be obtained:

$$H_{inside-slit}(y,z) = t_0 f_0(y,z), \quad (S2)$$

with the fundamental mode: $f_0(y,z) = (N_0)^{-1/2}\exp(-ikn_1z)$ ($|y| < w/2$) or 0 ($|y| \geq w/2$), (S3)

and the transmission mode: $t_0 = \frac{2(N_0/N_p)^{1/2}}{(n_1/n_2)w' I_0+1}$ (S4)

by matching the perfectly-conducting (PC) boundary conditions at z=0 due to the assumption of continuity of E_y and H_x,[4]and the reflection mode:

$$r_u = \delta(0) - t_0\left(N_0/N_p\right)^{1/2} w' \frac{n_1}{n_2(1-u^2)^{1/2}}, \quad \text{(S5)}$$

where δ represents the Dirac distribution,[5] w' represents the normalized width, and the normalization constants N_0 and N_p for the power flow on the slit aperture being unitary are given by $N_0=w/(2\varepsilon n_2)$ and $N_p= w/(2\varepsilon n_1)$, respectively.[1]

Python Numerical Calculations were used for solving the semi-analytical model, and the calculated I_0 and I_1 at designed w' are summarized in table S1-S4.

Note that I_0 and I_1 could also be changed into I_0'(I_0''), and I_1'(I_1''), respectively. We just list one group of I_0 while different groups of I_1, since I_0 depends on w' while I_1 depends on both metal permittivity and w'.

Table S1. I_0 and I_1 for gold at different wavelengths when the refractive index n_1 is 1.45 (I_0 equals to each other for different λ)

		600nm ε=-10.21+ 1.43i	**700nm ε=-17.94+ 1.61i**	**800nm ε=-26.27+ 1.85i**	**900nm ε=-35.80+ 2.43i**	**1000nm ε=-46.05+ 3.11i**	**1100nm ε=-57.32+ 3.87i**	**1200nm ε= -68.98+ 4.68i**
W'	**I_0**	**I_1**	**I_1**	**I_1**	**I_1**	**I_1**	**I_1**	**I_1**
0.1	3.09-4.09i	-0.05-2.74i	0.20-2.84i	0.34-2.88i	0.43-2.91i	0.49-2.92i	0.54-2.93i	0.57-2.94i
0.2	2.94-2.61i	0.64-2.40i	0.92-2.45i	1.06-2.46i	1.16-2.47i	1.23-2.47i	1.28-2.47i	1.32-2.46i
0.3	2.72-1.69i	1.12-1.90i	1.40-1.87i	1.54-1.85i	1.64-1.83i	1.71-1.81i	1.76-1.80i	1.80-1.78i
0.4	2.43-1.05i	1.36-1.32i	1.61-1.23i	1.74-1.17i	1.82-1.12i	1.88-1.09i	1.92-1.06i	1.96-1.04i
0.5	2.13-0.64i	1.37-0.77i	1.57-0.62i	1.66-0.54i	1.72-0.48i	1.77-0.43i	1.80-0.39i	1.82-0.36i
0.6	1.82-0.34i	1.20-0.32i	1.32-0.16i	1.38-0.06i	1.42+0.01i	1.44+0.06i	1.45+0.10i	1.47+0.13i
0.7	1.54-0.18i	0.91-0.04i	0.97+0.12i	0.99+0.21i	1.00+0.27i	1.01+0.32i	1.01+0.36i	1.01+0.38i
0.8	1.30-0.10i	0.61+0.07i	0.62+0.20i	0.61+0.28i	0.60+0.32i	0.59+0.36i	0.58+0.38i	0.57+0.40i
0.9	1.11-0.06i	0.35+0.05i	0.33+0.13i	0.31+0.18i	0.29+0.21i	0.28+0.23i	0.27+0.24i	0.26+0.25i
1.0	0.97-0.07i	0.19-0.06i	0.17-0.02i	0.15-0.01i	0.13+0.00i	0.12+0.01i	0.11+0.01i	0.10+0.02i

Table S2. I0 and I1 for gold at different wavelengths when the refractive index n_1 is 1.0 (I_0 equals to each other for different λ)

		600nm ε=-10.21+ 1.43i	**700nm ε=-17.94+ 1.61i**	**800nm ε=-26.27+ 1.85i**	**900nm ε=-35.80+ 2.43i**	**1000nm ε=-46.05+ 3.11i**	**1100nm ε=-57.32+ 3.87i**	**1200nm ε= -68.98+ 4.68i**
w'	**I_0**	**I_1**	**I_1**	**I_1**	**I_1**	**I_1**	**I_1**	**I_1**
0.1	3.09-4.09i	0.27-2.89i	0.44-2.92i	0.53-2.93i	0.59-2.94i	0.63-2.94i	0.67-2.95i	0.69-2.95i
0.2	2.94-2.61i	0.99-2.48i	1.18-2.47i	1.27-2.47i	1.34-2.46i	1.39-2.46i	1.42-2.45i	1.45-2.45i
0.3	2.72-1.69i	1.48-1.89i	1.66-1.83i	1.75-1.80i	1.82-1.78i	1.86-1.76i	1.90-1.75i	1.92-1.74i
0.4	2.43-1.05i	1.69-1.22i	1.84-1.12i	1.92-1.06i	1.97-1.03i	2.01-1.00i	2.04-0.97i	2.06-0.96i
0.5	2.13-0.64i	1.63-0.60i	1.74-0.47i	1.79-0.40i	1.83-0.35i	1.85-0.31i	1.87-0.28i	1.89-0.26i
0.6	1.82-0.34i	1.37-0.12i	1.43+0.02i	1.45+0.09i	1.47+0.15i	1.48+0.18i	1.49+0.21i	1.49+0.24i
0.7	1.54-0.18i	1.00+0.16i	1.01+0.28i	1.01+0.35i	1.01+0.40i	1.00+0.43i	1.00+0.46i	1.00+0.48i
0.8	1.30-0.10i	0.62+0.24i	0.60+0.33i	0.58+0.38i	0.57+0.41i	0.56+0.44i	0.55+0.45i	0.54+0.47i
0.9	1.11-0.06i	0.33+0.16i	0.29+0.21i	0.27+0.24i	0.25+0.26i	0.24+0.27i	0.23+0.28i	0.22+0.28i
1.0	0.97-0.07i	0.16-0.01i	0.13+0.01i	0.11+0.01i	0.10+0.02i	0.09+0.02i	0.08+0.02i	0.07+0.02i

Table S3. I_0 and I_1 for gold at different wavelengths when the refractive index n_1 is 1.45 (I_0 equals to each other for different λ) with more detailed w' range

		600nm ε=-10.21+ 1.43i	**700nm ε=-17.94+ 1.61i**	**800nm ε=-26.27+ 1.85i**	**900nm ε=-35.80+ 2.43i**	**1000nm ε=-46.05+ 3.11i**	**1100nm ε=-57.32+ 3.87i**	**1200nm ε= -68.98+ 4.68i**
w'	**I_0**	**I_1**	**I_1**	**I_1**	**I_1**	**I_1**	**I_1**	**I_1**
0.02	3.14-7.35i	-0.73-2.86i	-0.49-2.98i	-0.37-3.03i	-0.29-3.06i	-0.23-3.08i	-0.19-3.09i	-0.16-3.10i
0.04	3.13-5.93i	-0.55-2.84i	-0.31-2.96i	-0.19-3.01i	-0.10-3.04i	-0.05-3.06i	-0.00-3.07i	0.03-3.08i
0.06	3.12-5.19i	-0.37-2.82i	-0.13-2.93i	-0.01-2.98i	0.08-3.01i	0.14-3.02i	0.18-3.04i	0.22-3.04i
0.08	3.11-4.54i	-0.21-2.79i	0.04-2.89i	0.17-2.94i	0.25-2.96i	0.32-2.98i	0.36-2.99i	0.40-3.00i
0.12	3.07-3.73i	0.10-2.69i	0.36-2.78i	0.50-2.82i	0.59-2.84i	0.65-2.85i	0.70-2.86i	0.74-2.86i
0.14	3.04-3.37i	0.25-2.63i	0.52-2.71i	0.65-2.74i	0.75-2.76i	0.81-2.77i	0.86-2.78i	0.90-2.78i
0.16	3.01-3.07i	0.39-2.56i	0.66-2.63i	0.80-2.66i	0.89-2.67i	0.96-2.68i	1.01-2.68i	1.05-2.68i
0.18	2.98-2.81i	0.52-2.49i	0.79-2.54i	0.94-2.56i	1.03-2.57i	1.10-2.58i	1.15-2.58i	1.19-2.58i
0.22	2.90-2.39i	0.76-2.31i	1.04-2.34i	1.18-2.35i	1.28-2.35i	1.35-2.35i	1.40-2.34i	1.44-2.34i
0.24	2.86-2.18i	0.86-2.22i	1.14-2.23i	1.29-2.23i	1.39-2.23i	1.46-2.22i	1.51-2.22i	1.55-2.21i

Table S4. I_0 and I_1 for gold at different wavelengths when the refractive index n_1 is 1.0 (I_0 equals to each other for different λ) with more detailed w' range

		600nm ε=-10.21+ 1.43i	**700nm ε=-17.94+ 1.61i**	**800nm ε=-26.27+ 1.85i**	**900nm ε=-35.80+ 2.43i**	**1000nm ε=-46.05+ 3.11i**	**1100nm ε=-57.32+ 3.87i**	**1200nm ε= -68.98+ 4.68i**
w'	**I_0**	**I_1**	**I_1**	**I_1**	**I_1**	**I_1**	**I_1**	**I_1**
0.02	3.14-7.35i	-0.44-3.02i	-0.28-3.07i	-0.20-3.09i	-0.14-3.10i	-0.10-3.11i	-0.07-3.12i	-0.05-3.12i
0.04	3.13-5.93i	-0.26-3.01i	-0.09-3.05i	-0.01-3.07i	0.05-3.08i	0.09-3.09i	0.12-3.09i	0.15-3.10i
0.06	3.12-5.19i	-0.08-2.98i	0.09-3.02i	0.18-3.03i	0.24-3.05i	0.28-3.05i	0.31-3.06i	0.33-3.06i
0.08	3.11-4.54i	0.10-2.94i	0.27-2.97i	0.36-2.99i	0.42-3.00i	0.46-3.01i	0.49-3.01i	0.52-3.01i
0.12	3.07-3.73i	0.43-2.82i	0.60-2.85i	0.69-2.86i	0.76-2.87i	0.80-2.87i	0.84-2.87i	0.86-2.87i
0.14	3.04-3.37i	0.58-2.75i	0.76-2.77i	0.85-2.78i	0.92-2.78i	0.96-2.78i	1.00-2.78i	1.02-2.78i
0.16	3.01-3.07i	0.73-2.67i	0.91-2.68i	1.00-2.68i	1.07-2.68i	1.11-2.68i	1.15-2.68i	1.18-2.68i
0.18	2.98-2.81i	0.86-2.58i	1.05-2.58i	1.14-2.58i	1.21-2.58i	1.26-2.58i	1.29-2.57i	1.32-2.57i
0.22	2.90-2.39i	1.11-2.37i	1.30-2.36i	1.39-2.35i	1.46-2.34i	1.51-2.33i	1.54-2.32i	1.57-2.32i
0.24	2.86-2.18i	1.22-2.26i	1.40-2.23i	1.50-2.22i	1.57-2.21i	1.61-2.20i	1.65-2.19i	1.68-2.18i

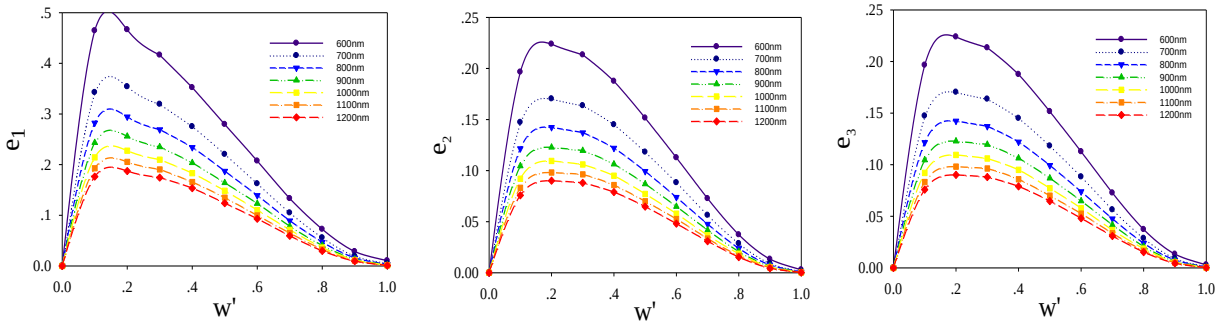

(a) (b) (c)

Fig. S1. Quantitative correlation of SPP generation efficiencies e to incident wavelength and the scaled slid width at the nanoledge interfaces. (a) Au/quartz interface in air; (b) Au/air interface in the nanoledge; (c) Au/air interface at the top of nanoledge.

Factor analysis:

The following equations are applied for the factor analysis:[6]

$$b_j = a_1 a_2 \dots a_p, \quad \text{(S6)}$$

$$c_k = b_1 b_2 \dots b_q, \quad \text{(S7)}$$

$$\mu(a_i/b_j) = \frac{\text{No.of } a_i}{\sum_{i=1}^{n=p} \text{No.of } a_i}, \quad \text{(S8)}$$

$$\mu(b_j/c_k) = \frac{\text{No.of } b_j}{\sum_{j=1}^{n=q} \text{No.of } b_j}, \quad \text{(S9)}$$

$$\mu(a_i/c_k) = \sum_{j=1}^{n=q} \mu(a_i/b_j)\mu(b_j/c_k), \quad \text{(S10)}$$

where p and q represents the number of observable random variables (here are w_1 or w_2, λ, n_1, $n_2/n_3/n_4$); μ(m/n) represents the influence factor coefficient of m on the calculation of n. With some acceptable algorithm approximation assumptions,[7] such as (sin(q))~(q), (\)~(*), and (t+1)~t.

Based on the factor analysis, below is the scheme of the relationship between independent variables (factors) (w, λ, $n_2/n_3/n_4$, n_1) and resulted parameters (w', I_0, I_1, e, v, and ϵ).

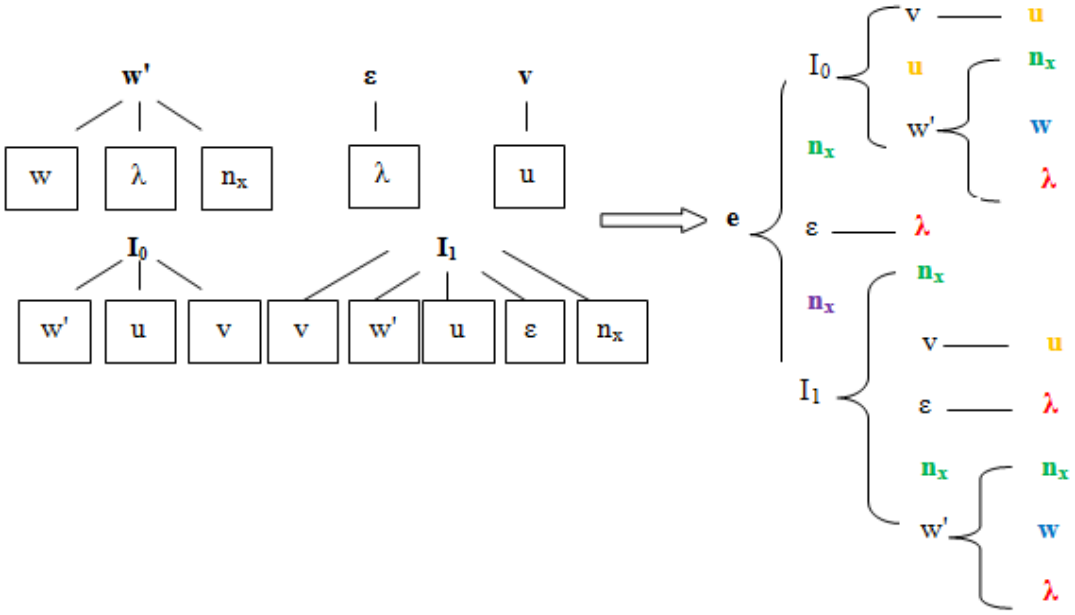

Fig. S2. The relationships between the factors of w, λ, $n_2/n_3/n_4$, n_1 and u on w', I_0, I_1, e, v, and ϵ, respectively.[6]

The factor analysis data for Figure 3 as part codes for Matplotlib

```
data = {
  'column names':
    ['w_norm', 'I0', 'I1', 'e', 'gamma_u', 'epsilon'],
  'a':
    [[0.34, 0.15, 0.12, 0.12, 0.00, 0.00],
     [0.33, 0.15, 0.17, 0.20, 0.00, 1.00],
```

```
        [0.00, 0.00, 0.00, 0.13, 0.00, 0.00],
         [0.33, 0.15, 0.24, 0.28, 0.00, 0.00],
         [0.00, 0.55, 0.47, 0.27, 1.00, 0.00]],
    'b':
        [[0.34, 0.15, 0.12, 0.13, 0.00, 0.00],
         [0.33, 0.15, 0.17, 0.23, 0.00, 1.00],
        [0.33, 0.15, 0.24, 0.32, 0.00, 0.00],
        [0.00, 0.00, 0.00, 0.00, 0.00, 0.00],
         [0.00, 0.55, 0.47, 0.32, 1.00, 0.00]],
    'c':
        [[0.34, 0.15, 0.12, 0.12, 0.00, 0.00],
         [0.33, 0.15, 0.17, 0.22, 0.00, 1.00],
        [0.16, 0.07, 0.12, 0.23, 0.00, 0.00],
         [0.17, 0.08, 0.12, 0.14, 0.00, 0.00],
         [0.00, 0.55, 0.47, 0.29, 1.00, 0.00]],
    'd':
        [[0.34, 0.34, 0.23, 0.17, 0.00, 0.00],
         [0.33, 0.33, 0.32, 0.31, 0.00, 1.00],
        [0.16, 0.16, 0.22, 0.32, 0.00, 0.00],
         [0.17, 0.17, 0.23, 0.20, 0.00, 0.00],
         [0.00, 0.00, 0.00, 0.00, 0.00, 0.00]]}
return data
```

FDTD simulations:

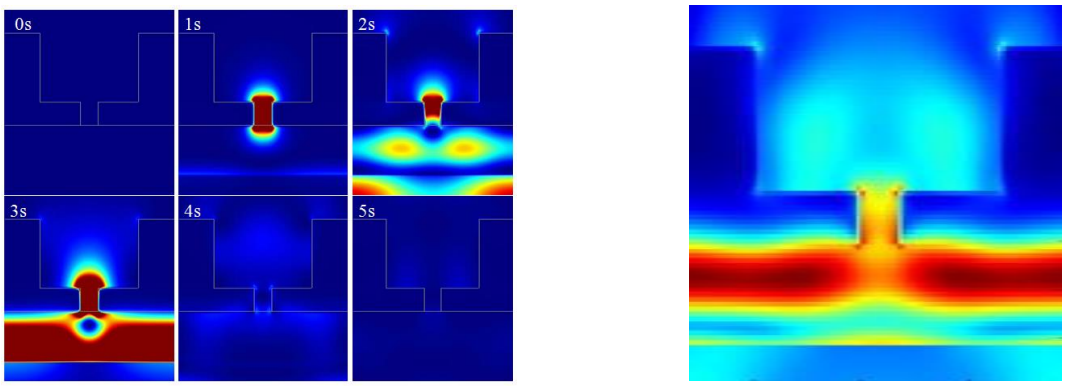

(a) (b)

Fig. S3. (a) Movie screenshots of the TE field propagation through the simulation volume of 280-50 nm nanoledge system are shown; (b) the corresponding TM field distributions of the 280-50 nm nanoledge system

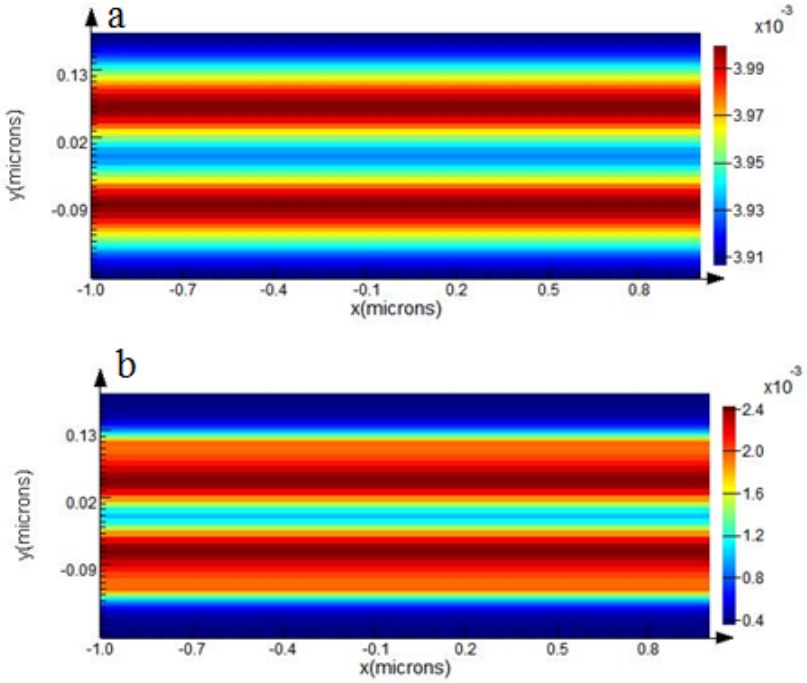

Fig. S4. FDTD calculated magnetic (TM) field distribution (near field) on the reflected (a) and transmitted side (b).

Table S5 Maximum Transmission of w_2-w_1 nanoslit systems with different w_1 and w_2.

w_1 (nm)	**w_2 (nm)**					
	300	280	260	240	220	200
100	0.220	0.208	0.190	0.171	0.151	0.132
90	0.228	0.215	0.199	0.180	0.161	0.142
80	2.231	0.221	0.207	0.191	0.172	0.154
70	0.229	0.223	0.213	0.200	0.185	0.168
60	0.256	0.238	0.217	0.203	0.193	0.181
50	**0.283**	0.270	0.251	0.231	0.208	0.185
40	0.279	0.274	0.266	0.255	0.241	0.225
30	0.194	0.199	0.202	0.203	0.204	0.204
20	0.121	0.118	0.114	0.110	0.106	0.103
10	0.023	0.020	0.018	0.016	0.014	0.013

Table S6. The SPP generation efficiency e_1, e_2, e_3 for the nanoledge geometry w_2/w_1 of 280nm-50nm.

$n_2=n_3=n_4$	e_1	e_2	e_3	Δe
1	0.4791	0.1806	0.1613	0
1.1	0.4223	0.2123	0.1589	-0.0275
1.2	0.3821	0.2508	0.1542	-0.0339
1.3	0.3407	0.2823	0.1498	-0.0482
1.4	0.3107	0.3158	0.1426	-0.0519
1.5	0.2803	0.3483	0.1306	-0.0618

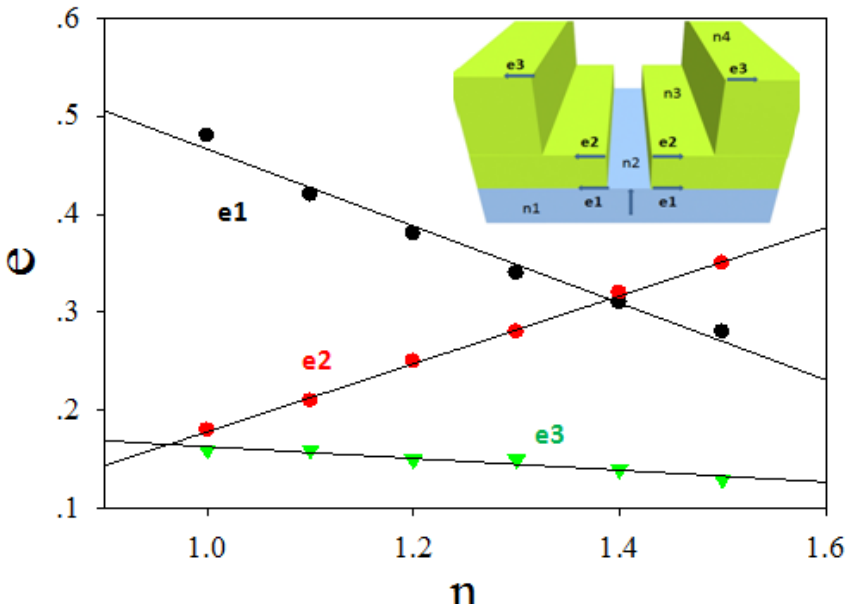

Fig. S5. Individual SPP generation efficiency of the three interfaces of nanoledge with w_2/w_1 280nm-50 nm as a function of refractive index $n_2=n_3=n_4$, n1 is 1.45 for quartz.

Nanofabrication and optical measurements:

Focused Ion Beam Fabrication of Nanoledge Structures: Quartz slides (25×25 mm^2) were used as the substrate for sample preparation. These were rinsed first with acetone in an ultrasonic bath for 10 min, and then rinsed with deionized water and dried under a nitrogen stream. Then the slides were placed on a hot plate with the temperature set at 180 ^{0}C to remove any traces of water remaining. These slides were exposed to an oxygen plasma for 300 s at a pressure of 200 mTorr to remove organic contaminants on the surface. A 250 nm thin layer of gold (99.95%, Alfa Aesar, USA) was evaporated onto the cleaned quartz slides at around 2.0×10^{-6} Torr, at a deposition rate of 0.2 nm s^{-1} in an electron beam evaporator. A 2.5 nm layer of titanium was first coated before the gold to promote adhesion to the substrate. These gold films were stored under nitrogen in sealed vials prior to FIB milling. The fabrication of the nanoledge structure was done using a dual-beam focused ion beam system (Seiko Instruments SMI3050SE). The focused ion beam column was equipped with a Ga^+ source and operated at 30 keV under a 5 pA beam current. The nanoledge structure measured ~50 nm wide in the Au-quartz interface and ~250 nm wide in the Au-air interface, with a slit length of 30 μm. A vector scan with different line densities were used to introduce different etching depths into the Au film to obtain different widths in the two interfaces. The total area of the array was maintained to be 30×30 μm^2.

Fig S6. – Schematic of FIB milling routine employed for fabricating the nanoledge structure. a) Cleaning the substrates b) Thin metal film deposition c) FIB milling of the targeted nanoledge structure.

Electron Beam Lithography Fabrication of Nanoledge Structures: Electron beam lithography (EBL, Raith e-Line) was used for the fabrication of Au nanoledge structures in arrays (30×30 μm^2). Three consecutive EBL steps were followed to achieve the final structure as described as follow. The fabrication scheme is illustrated in Fig S7.

Conductive indium tin oxide coated glass slides (ITO) (Delta's Technologies) were used as the substrates to minimize charging during the fabrication. ITO substrates were rinsed using three solvents: acetone, methanol and iso-propanol; ultrasonication was done in each solvent for 5 min. The ITO substrates were rinsed with DI water and dried with a nitrogen stream. These substrates were baked at 180 ^oC for 2 min to remove any moisture from the surface. In step one, as illustrated Fig S7 (a), poly-methyl-methacrylate (950 A4 PMMA, Microchem) was spun on the substrate at a speed of 1500 rpm for 40 s using a spin processor (Laurell *WS-400-6NPP-LITE*) and baked on a hot plate at 180 ^0C for 5 min. EBL was performed at an acceleration voltage of 20 keV and with an exposure dose of 300 $\mu C/cm^3$ using a 7.5 μm aperture to write the markers on PMMA in order to define the coordinate system on the substrate which will act as the reference on the subsequent steps. The sample was then developed for 90 s in a developing solvent consisting of methyl isobutyl ketone and isopropanol in a 3:1 ratio to dissolve the exposed PMMA. Then gold was evaporated on to this sample to a thickness of 50 nm, with a 5 nm of Titanium to help the Au to better adhere to the substrate. The rate of evaporation was maintained at 0.3 Å s^{-1} to allow smooth deposition of the metal. After the metal deposition, the samples were kept overnight in acetone to remove the remaining PMMA resist.

In step 2 (Fig S7 (b)), the substrate with the coordinates obtained from step one was taken and rinsed with acetone, methanol, iso-propanol: 3 minutes in each solvent, in order to remove any dirt particles on the substrate. The substrates were then dried with a nitrogen stream and baked at 90 ^0C for 4 min to remove any moisture from the surface. Negative e-

beam resist (maN 2403, Micro Resist Technologies) was spun on the substrates at a speed of 3000 rpm for 30 s using the spin processor to obtain a final film thickness of 300 nm. The resist-coated substrates were baked for 60 s on a hot plate at 90 ^{o}C. Then the resist–coated substrates were placed under the EBL system to make the 80 nm width nano-slits. Electron beam exposure was performed at an acceleration voltage of 20 keV using the 7.5 μm with an exposure dose of 100 μC/cm^{3}. The samples were developed using an alkaline developing solution (CD-26, MicroChem) for 90 s to dissolve the unexposed resist. Gold (Au) was evaporated on to the sample at a thickness of 50 nm, with a 5 nm Ti layer to promote adhesion. After the metal deposition, the remaining resist was removed by soaking in Remover PG 1165 under 90 ^{o}C for about 60 min followed by 5 min sonication.

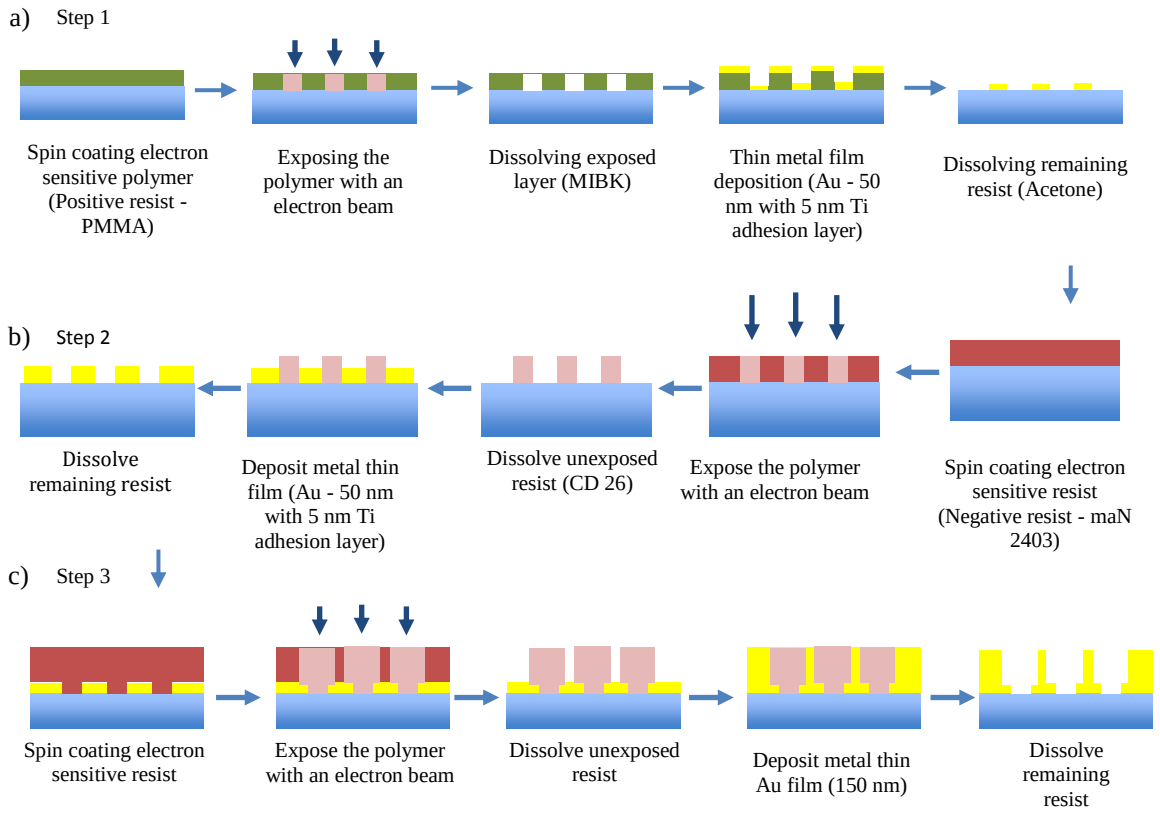

Fig. S7. Schematic of steps followed in fabricating the Nanoledge structures using Electron Beam Lithography. a) Step 1 - Fabrication of alignment markers on the substrate b) Step 2 - Fabrication of 50 nm width slits using negative e-beam resist c) Step 3 – Alignment and fabrication of the 250 nm width slit on top of the bottom 50 nm slit to obtain the intended nanoledge structure.

In step three (Fig S7 (c)), the sample prepared in step 2 was taken and cleaned as previously described. The negative e-beam resist was spun coated as before with the same conditions and baked for 1 min in a hot plate at 90 ^{o}C. The samples were again placed under the EBL system and the same exposure parameters were used as similar to step two. With the help of the pre-defined coordinates the second nanoslit array was overlaid right on the 80 nm nanoslit array. After the exposure, the sample was developed using the CD 26. Gold was deposited to a thickness of 150 nm. Lift-off of the remaining resist was performed as similar to step 2 in order to obtain the final nanoledge structure.

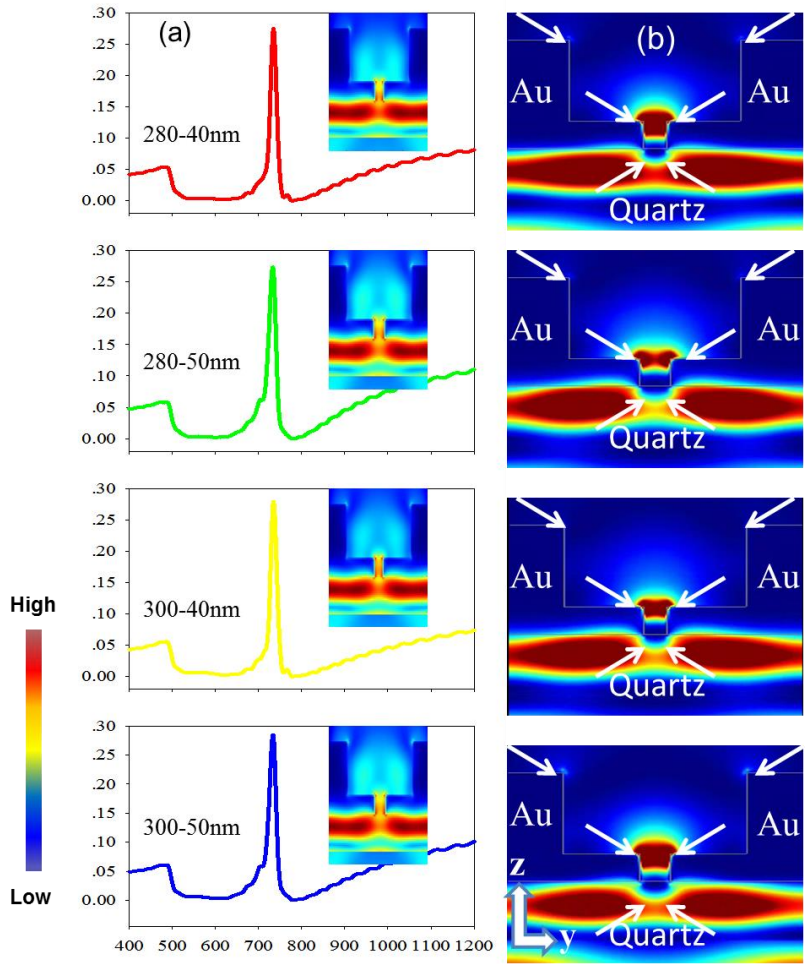

Fig. S8. Panel (a) shows the calculated transmission spectra of the four w_2-w_1 nanoledge systems with the TM field profiles illustrated in the insets. Panel (b) the corresponding TE field dynamics at 3 seconds calculated for the four nanoledge systems.

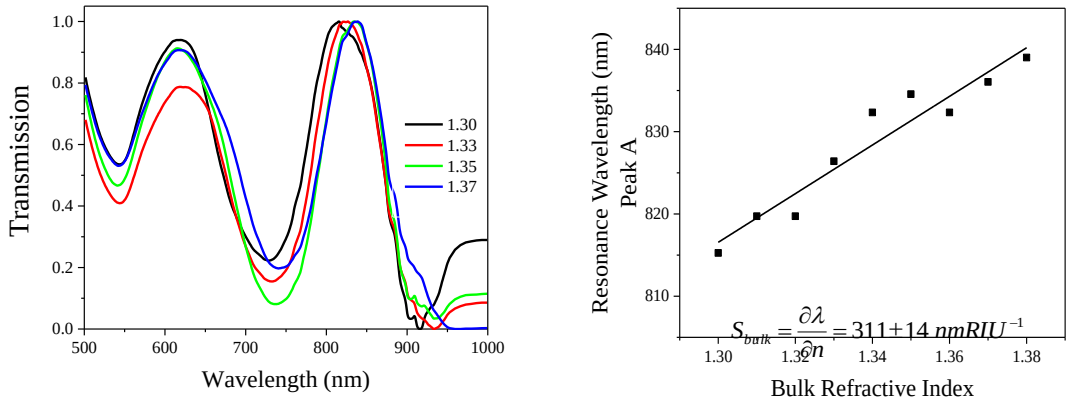

Fig. S9. Refractive index sensitivity measurements of EBL Fabricated nanoledge (see main Fig. 6a) were obtained by recording the transmission spectra of the nanoledges while changing the refractive index of the outside medium by using refractive index standards as illustrated in (a). Resonance wavelength of the peak A is plotted versus the refractive index in (b). Three lines depict the refractive index response of three different arrays of nanoledges. The slope of the lines gives the refractive index sensitivity which was calculated to be 311 nmRIU^{-1} and standard deviation of the refractive index sensitivity between the three arrays is given as the error of this measurement.

Reference:

1. Lalanne, P.; Hugonin, J. P.; Rodier, J. C. *J. Opt. Soc. Am. A* **2006,** 23, (7), 1608-1615.
2. Wei, P.-K.; Chou, H.-L.; Cheng, Y.-R.; Wei, C.-H.; Fann, W.; Tegenfeldt, J. O. *Optics Communications* **2005,** 253, (1–3), 198-204.
3. Xie, Y.; Zakharian, A.; Moloney, J.; Mansuripur, M. *Opt. Express* **2004,** 12, (25), 6106-6121.
4. Lalanne, P.; Hugonin, J. P.; Rodier, J. C. *Physical Review Letters* **2005,** 95, (26), 263902.
5. DuBridge, L. A. *Physical Review* **1933,** 43, (9), 727-741.
6. Kline, P., *An easy guide to factor analysis*. Taylor and Francis: Hoboken, NJ, 2014; p 203.
7. Vazirani, V. V., *Approximation Algorithms*. Springer-Verlag: Berlin Heidelberg, 2003; p 380.